Evidence of emerging Griffiths singularity in La$_{0.5}$ Sr$_{0.5}$ MnO$_3$ nanocrystalline probed by magnetization and electron paramagnetic resonance

Xiyuan Zhang [a], Jiyu Fan [a, *], Lisa Xu [a], Wei Tong [b], Dazhi Hu [a], Xun He [c], Lei Zhang [b], Li Pi [b], Yuheng Zhang [b]

[a] Department of Applied Physics, Nanjing University of Aeronautics and Astronautics, Nanjing 210016, China
[b] High Magnetic Field Laboratory, Chinese Academy of Sciences, Hefei 230031, China
[c] College of Environmental Science and Engineering, Hunan University, Changsha 410082, China

HIGHLIGHTS

- Griffiths singularity rather than superparamagnetism occurs in La$_{0.5}$Sr$_{0.5}$MnO$_3$ nanoparticals.
- The sample's size reduced to nanoscale results in the short-range ferromagnetic interaction.
- The core-shell model is used to understand the formation of Griffiths phase in nanometer La$_{0.5}$Sr$_{0.5}$MnO$_3$.

ARTICLE INFO

ABSTRACT

We present an investigation of Griffiths singularity in La$_{0.5}$ Sr$_{0.5}$ MnO$_3$ nanocrystalline by means of magnetic susceptibility and electron paramagnetic resonance (EPR). An unusual platform was found in paramagnetic region. Based on the analysis of EPR spectrum and magnetization variation across the whole temperature range of phase transition, we confirm it is due to the presence of Griffiths singularity rather than a superparamagnetic state in the nanocrystalline system. Such a singularity phase is constituted with some correlated ferromagnetic clusters which embed in paramagnetic matrix. Although they form ferromagnetic spin correlation, the system do not yield any spontaneous magnetization. According to core—shell model, the emergence of Griffiths singularity can be considered due to the presence of local ferromagnetic fluctuations originated from surface spin disorder as the sample size is confined to nanoscale.

1. Introduction

Perovskite manganites R$_{1-x}$ A$_x$MnO$_3$ (R = rare earth element, A = divalent alkaline earth element) have attracted much attention due to the richness of emergent phenomena, including colossal magnetoresistance, charge ordering, and multiferroics [1—6]. A hallmark of these complex materials is the strong coupling between the structural, electronic and magnetic properties. A small change in one property can cause a large change in another property. For instance, Zhai et al. found that, by spatially confining epitaxial La$_{1-x}$ Pr$_x$Ca$_{3/8}$ MnO$_3$ thin film to the nanoscale, the

electronic transport lanes are forced to pass through both the low and the high resistance lanes [7]. This behavior differs from past investigation on bulk and films in which only the low resistance lanes is probed. Recently, Moya et al. reported that a giant and reversible extrinsic magnetocaloric effect La$_{0.7}$ Ca$_{0.3}$ MnO$_3$ thin film could be created be strain of BaTiO$_3$ substrates [8]. However, bulk La$_{0.7}$ Ca$_{0.3}$ MnO$_3$ and epitaxial film La$_{0.7}$ Ca$_{0.3}$ MnO$_3$ on SrTiO$_3$ substrates show small magnetocaloric effect at their Curie temperatures. In fact, a subtle balance between different phases generally hides behind these complex phenomena, which can be readily shifted or entirely broken by some external stimulus. Meanwhile, it also provide a precious opportunity for us to discover the potential properties and possible mechanism. In the early stage, perovskite manganites in the form of bulk and thin film have been extensively investigated. Therefore, the reduction in sample size to

* Corresponding author.
  E-mail address: jiyufan@nuaa.edu.cn (J. Fan).

nanometer level is an effective means to change this subtle balance and find out new phenomena due to the physical properties of nanomaterials strongly dependence on the size and shape of the nanocrystalline. As for perovskite manganites, the nanoscale materials exhibit numbers of unique properties, such as low field magnetoresistance, surface spin-glass and small saturation magnetization as compared to their corresponding bulk and thin film materials [9–13].

Generally, for the most bulk and thin film of hole-doping manganites, they always show paramagnetic behavior in high temperature regime. However, due to the magnetic properties dependence on the size of nanoparticles, at the nanoscale, each nanoparticle may contain only a single magnetic domain. Thus, the high temperature paramagnetic behavior is easily transformed to a superparamagnetic state since that the thermofluctuational motion of the particle magnetic moment may overcomes the magnetic anisotropy energy. Under this situation, the magnetization direction of particles shows a rapid fluctuation rather than a fixing direction. Therefore, exploration of high temperature paramagnetic state is an important topic for the nanoscale perovskite manganites. To shed light on this issue, in this paper we mainly study the high temperature magnetic behavior of $La_{0.5} Sr_{0.5} MnO_3$ nanoparticles. Polycrystalline bulk $La_{0.5} Sr_{0.5} MnO_3$ manganite is a typical ferromagnetic material, which shows a strong paramagnetic-ferromagnetic phase transition at $T_C = 317.3$ K [14]. Above T_C, the bulk ceramic show a normal paramagnetic state and the inverse susceptibility vs temperature curve can be fitted well with the Curie−Weiss law. Our results show that the nanoscale $La_{0.5} Sr_{0.5} MnO_3$ particles retain paramagnetic-ferromagnetic (PM-FM) phase transition. However, at high temperature region, different from bulk sample, the inverse susceptibility vs temperature curve can not be fitted by the Curie−Weiss law in the whole PM region but shows a distinct deviation at far above T_C. Moreover, the data of isothermal magnetization exclude the presence of proleptic superparamagnetic state in $La_{0.5} Sr_{0.5} MnO_3$ nanoparticles. By analyzing the results of electron paramagnetic resonance (EPR), we testified that the Griffiths phase existed in the nanoparticle sample instead of superparamagnetic state. The core−shell model was used to understand its emergence [15,16]. The strong competition between the increasing surface spin moments and the core magnetic moments is the main reason for it.

2. Experiment

Nanocrystalline $La_{0.5} Sr_{0.5} MnO_3$(LSMO) samples was prepared by the sol−gel method. The stoichiometric amounts of high-purity $La_2 O_3$, $SrCO_3$ and $MnCO_3$ were first converted into nitrates by adding nitric acid, forming a stable solution. The solution was then heated on a thermal plate under constant sintering at 100 °C for 24 h to remove the excess water and obtain a viscous gel. The obtained gel was decomposed at 400 °C and the resulting precursor powder was heated in air at 800 °C for 4h to obtain nanocrystalline sample. Phase purity and crystal structures were identified by X-ray diffraction (XRD) using Cu Kα radiation at room temperature. The microstructure for nanocrystalline sample was identified by scanning electron microscopy (SEM). The magnetic measurements were carried out using a commercial superconducting quantum interference device magnetic property measurement system. Temperature dependence of magnetization were measured with zero-field cooing(ZFC) and field cooling(FC) mode under the applied magnetic field 100 Oe. The EPR measurement of the powder sample was performed at selected temperatures using a Bruker EMX-plus model spectrometer with a heater operating at X-band frequencies ($\nu \approx$ 9.4 GHz).
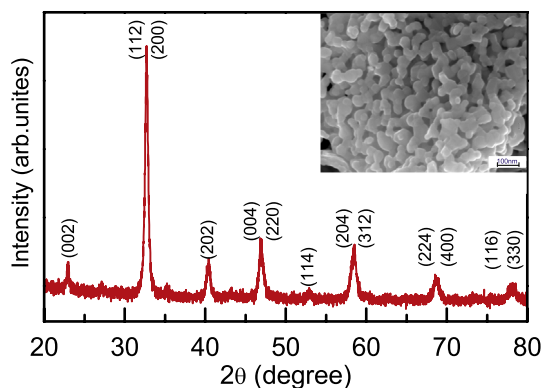

Fig. 1. The XRD patterns of nanocrystalline $La_{0.5} Sr_{0.5} MnO_3$. Inset shows SEM micrographs of nanocrystalline sample.

3. Results and discussion

XRD patterns of nanoparticle LSMO samples are shown in Fig. 1. According to the standard JCPDS cards, the peaks were indexed corresponding to orthorhombic perovskite structure with space group *Pnma*. The inset of Fig. 1 shows the SEM micrograph of the nanocrystalline LSMO. By analyzing the size distribution, one can find that the average sizes of particles are about 100 nm. The particles size can be further confirmed by Scherrer formulation $D = k\lambda/(\beta cos2\theta)$, where D is the diameter of the particle, k (0.89) is the particle shape factor, λ(0.15406 nm) is the wavelength of Cu Kα radiation, β and θ are the peak full width at half maximum (FWHM) and the diffraction angle of XRD (112) peak, respectively. The obtained average particle size is about 88.6 nm, basically consistent with the size observed from SEM in limits of errors. Hence, the nanocrystalline particles can be thought to correctly form the desired $La_{0.5} Sr_{0.5} MnO_3$ phase with average size of 100 nm.

Temperature dependence of dc magnetization of nanocrystalline LSMO in the FC mode under an applied field of 100 Oe is plotted in Fig. 2(right axes). Different from a sharp PM-FM transition observed in our previous bulk LSMO, [14], the sample shows a broader PM-FM transition. Moreover, note that the PM-FM transition can be roughly separated into three parts, T> 375 K, 375 K > T> 358 K, and T < 358 K. At T > 375 K, the magnetization almost remains unchanged with the decrease of temperature,
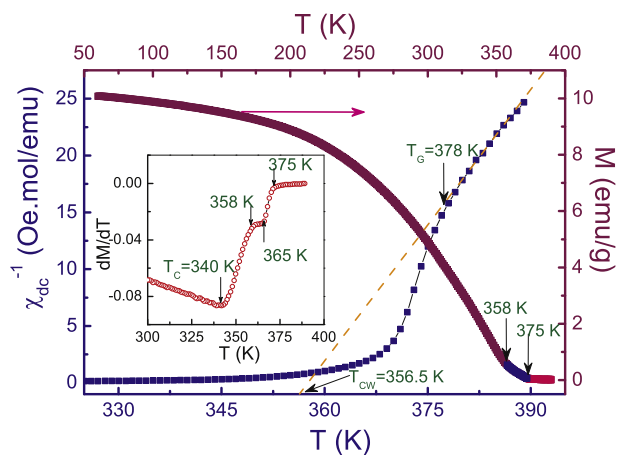
Fig. 2. Temperature dependent inverse susceptibility χ^{-1} (left) and magnetic susceptibility for nanocrystalline $La_{0.5} Sr_{0.5} MnO_3$ measured under an applied field of 100 Oe (right). The dash line represents the linear fitting according to Curie−Weiss law. Inset shows the plots of dM/dT vs T.

corresponding to PM state. At T < 358 K, the magnetization shows a sharp increase implying an appearance of FM state. Thus the temperature range of 358 K < T< 375 K is considered to be a transitional region. The Curie temperature T_C, defined by the minimum in dM/dT curve, has been determined to be 340 K (see the inset of Fig. 2). In the inset, an unusual platform can be observed in 358 K < T< 365 K. Generally, as magnetic systems are in a pure PM state their dM/dT curves show a continuous curve at T > T_C. Here, the existence of platform implies a possible deviation of PM state above 340 K. Many factors including FM cluster, spin fluctuation, and quenched disorder can cause this deviation. In order to discern the reason, Fig. 2(left axes) shows the temperature dependence of the inverse susceptibility ($\chi^{-1} = H/M$) and the fitting results (dashed line) according to the Curie–Weiss law $\chi = C/(T-T_{CW})$, where C is the Curie constant and T_{CW} is Weiss temperature. At T > 378 K, the relation between susceptibility χ^{-1} and temperature T preferably follows the Curie–Weiss law. However, at T < 378 K, a sharp downturn is observed much above 340 K. The deviation of the inverse susceptibility from the high-temperature straight line indicates the onset of the magnetic interaction between magnetic moments [17]. This downturn allows us to argue the possible existence of Griffiths singularity because the smeared phase transition gives rise to an upward curvature in inverse susceptibility $\chi^{-1}(T)$ curves above T_C [18]. Moreover, the similar signature of Griffiths phase has been also observed in other manganites [19–22].

Here, for magnetic nanoparticles, however, the emergence of superparamagnetic behavior need to be considered. In the field of superparamagnetic discussion, blocking temperature (T_b) is an important characteristic value that the thermal energy overcomes the magnetic anisotropy energy. At T > T_b, the magnetization direction of nanoparticles follows the direction of the applied field. On the contrary, at T < T_b, the thermal energy is less than the magnetic anisotropy energy, hence the direction of magnetization of each particles only lies in the direction of easy axis. As the temperature is decreased, the systemical total magnetization is reduced since that the particles easy axes are randomly oriented. Thus, the magnetic anisotropy axes of the ZFC particles remain randomly oriented whereas those of the FC particles are preferentially oriented along the magnetic field applied in the course of cooling. As a result, the ZFC and FC curves generally show a noticeable bifurcation at blocking temperature. As shown in Fig. 3, both curves almost overlap completely and do not present any bifurcations, indicating that it is a typical PM-FM phase transition rather than superparamagnetism. Moreover, the evidence of the

presence of superparamagnetic state in this sample can be further examined from the data on field dependence of the magnetization at some constant temperatures. For a superparamagnet one expects the presence of hysteresis and remanence in M vs. H curves below T_b, but the absence of such effects above T_b. The inset of Fig. 3 shows two M vs. H curves measured at 5.0 and 370.0 K. For T = 370.0 K, the M vs. H curve does not readily appear to approach a saturated magnetization, but instead linearly increase as a function of H at the highest fields 3.0 T. In contrast, at T = 5.0 K, the M vs. H curve also does not show a noticeable hysteresis and remanence. Obviously, the unusual platform occurred on M(T) curve does not originate from the superparamagnetic state in nanoparticle LSMO sample. Therefore, the Griffiths phase naturally becomes the focus of our investigation.

The Griffiths phase is originally proposed in a diluted Ising ferromagnet where a fraction of sites are occupied by the magnetic moments but the rest are replaced by nonmagnetic ones or vacancy [23]. In this scenario, the nearest-neighbor exchange interaction with strength J and 0 are distributed randomly with probability p and (1-p), respectively. As p < p_c, there are no any long-range FM ordering to occur in the system (p_c denotes the percolation threshold). As p_c < p< 1, the system develops some long-range FM orderings at a related lower temperature $T_C(p)$ comparing with the temperature of establishing long-range FM interaction in an undiluted system of p = 1. In fact, the existence of Griffiths phase means the presence of nanoscale magnetic inhomogeneities in the PM background. In our previous study on bulk LSMO, none of Griffiths phase was observed [14]. Generally, the quenched disorder is prerequisite for presence of Griffiths phase. In manganite, the disorder mainly stems from random size distribution of cations on A/B sublattices. Moreover, due to the existence of Jahn-Teller active Mn^{3+} ions, they cause the localized lattice distortion which changes the Mn–O–Mn bond angle and length, inducing bond disorder for the magnetically active Mn–O–Mn network. Besides, the chemical substitution at Mn crystallographic sites is also another important factor for the formation of disorder. Obviously, for the current nanoparticle LSMO, this factor can be excluded. Due to without any reported Griffiths phase in bulk LSMO sample and the improvement of chemical and structural homogeneity of nanoparticles as compared with corresponding bulk counterpart, the former reasons can be also unconsidered. Therefore, the presence of Griffiths phase in the nanoparticle LSMO is undoubtedly related to the nanosized process for sample.

To further understand the presence of Griffiths phase, we performed the EPR measurement on the nanocrystalline LSMO sample. EPR is known as a powerful probe of spin dynamics and magnetic correlation in perovskite manganites on a microscopic level. Many investigations about spin-lattice coupling and spin–spin relaxation in bulk manganites have been reported by means of EPR [24–28]. In addition, the detailed EPR analysis of nano-crystals has been also reported [29]. Not only that, EPR is an important tool to probe electronic phase separation and Griffiths phase in perovskite manganites [30]. Deisenhofer et al. reported the directed observation of Griffiths phase in paramagnetic $La_{0.875} Sr_{0.125} MnO_3$ single crystals by using EPR [19]. As shown in Fig. 4(a), a series of EPR spectra (dP/dH) from 440 to 300 K across the phase transition regime are measured. At T ≥ 390 K, a single resonance line with a Lorentzian shape is shown in the inset of Fig. 4(a). The presence of single paramagnetic resonance lines just corresponds to the paramagnetic state in M(T) curves. Once T < 390 K, the resonance field gradually moves to low field regime, just corresponding to a tiny upward at 375 K on M(T) curve. As it is known, the shift to low field region implies the onset of internal ferromagnetic field formation. That is to say, some localized short-range FM couplings have appeared. As we know, the FM interaction in hole-doping
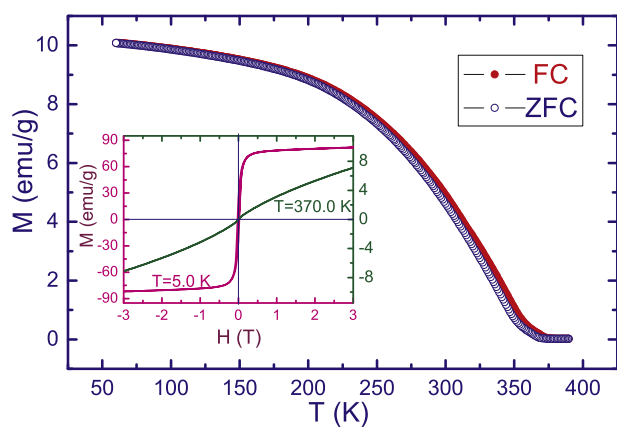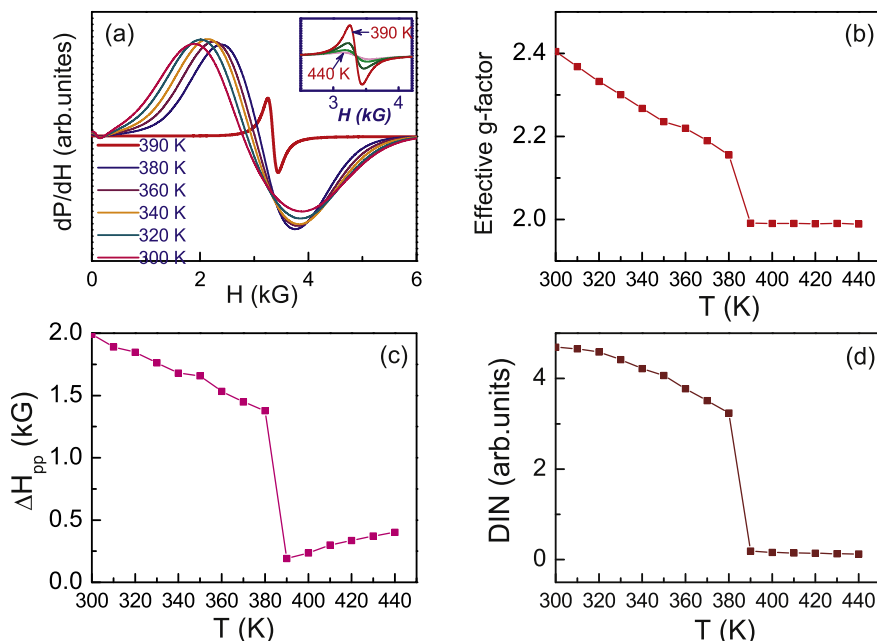

Fig. 3. Temperature dependence of magnetization measured at H = 100 Oe for ZFC (open circle) and FC(solid circle) mode and inset shows the isothermal magnetization measured at 5.0 and 370.0 K.

Fig. 4. (a) EPR spectrum of nanocrystalline $La_{0.5}$ $Sr_{0.5}$ MnO_3 at temperatures of 300 K≤ T≤ 440 K. (b, c, d) Temperature dependent effective g-factor, peak–peak width, and DIN, respectively.

manganites originates from the double exchange interaction between Mn^{3+} and Mn^{4+} ions. Although the present ratio $Mn^{3+}:Mn^{4+}$ was fixed to be 1:1, the actual ferromagnetism was affected strongly by A-site average cationic radius $\langle r_A \rangle$ which is related to the Mn−O−Mn bond angle and the hopping integral of e_g electron ($t_{ij\infty}$ $cos(\theta_{ij}/2)$) [3,5]. Obviously, $\langle rA \rangle$ = 1.263 in the present half-doping x = 0.5 component has deviated from $\langle r_A \rangle$ = 1.244 in x = 0.33 component $La_{0.67}$ $Sr_{0.33}$ MnO_3 which shows the optimal ferromagnetism [1,2]. Additionally, the ferromagnetism will be further suppressed as the sample's size is reduced to nanoscale. Therefore, in the current sample, LSMO nanoparticles are more inclined to form short-range rather than long-range interaction.

With further decreasing temperature, the EPR lines not only progressively shift towards low filed region but also show a distinct broadening. In fact, such a behavior is commonly observed for most perovskite manganites with PM-FM phase transition [31−35]. Except for the broadening PM resonance lines, they also show a large distortion and deviate from Lorentzian line shape at T< T_C. However, different from the common feature, as shown in Fig. 4(a), these PM resonance lines almost remain unchanged and reveal Lorentzian shape at T< 340 K, indicating that there are many residual PM ions in the entity even though the system has produced PM-FM phase transition. Magnetic phase transition can be identified by the change of effective g-factor with the formula $g = h\nu/\mu_B H_{res}$ (h is the Plank constant; ν is the frequency of the microwave; μ_B is the Bohr magnetor). Fig. 4(b) gives the effective g-factor as a function of temperature. As temperature decreases from 440 K to 390 K, the g value is close to 2 and shows a weak temperature dependence. However, at T = 380 K, the g value shows a sharp increase and then abidingly becomes larger until T = 300 K. In paramagnetic region, the temperature independent value of g-factor is generally close to 2, which is typical for Mn^{4+} in the MnO_6 octahedron coordination. On the contrary, in ferromagnetic region, it normally deviates from 2 since that the g-factor is often influenced by other coupling with spins. The above abrupt increase of g value implies that the large change of spin−orbit coupling constant at 380 K due to the formation of orbital ordering which influences the crystal field splitting and hence leads to an increase in the g

value. Similar to the variation of g-factor, in Fig. 4(c), the EPR linewidth ΔH_{PP} also shows an abrupt increase at the same temperature 380 K, which is very close to the onset (T = 378 K) of downward deviation in the inverse susceptibility $1/\chi(T)$ curve. According to Huber's theory, the variation of the EPR linewidth dependence on temperature was attributed to the exchange interaction between the magnetic ions and the lattice vibrations in paramagnetic region [36,37]. Namely, the temperature dependence on EPR linewidth is mainly determined by the ion−ion spin relaxation. For manganite, on approaching T_C from high temperature, the EPR linewidth generally shows a linear decrease upon the temperature due to the lengthening spin relaxation time. As T< T_C, the EPR linewidth of ferromagnetic region displays an increase. In fact, Fig. 4(c) also shows a linear decrease dependence on temperature from 440 to 390 K. Here, this obvious ascent at 380 K implies the presence of short ranged finite size FM clusters in PM region. For further understanding the above variation, we use the double-integrated intensity (DIN) to analyze the intensity of EPR spectra because it is an important parameter to identify the magnetic ion contribution to the resonant entities. Similar to the results of effective g-factor and linewidth ΔH_{PP}, a remarkable variation of DIN also occurs in the same temperature of 380 K. Above 390 K, the DIN almost remains unchanged. However, at T≤ 380 K, an enlarged DIN value occurs in Fig. 4(d) indicating that there are some extra magnetic ions which provide contribution to the EPR spectra. This point is consistent with the previous analysis on ΔH_{PP}, where ΔH_{PP} variation implies the form of FM clusters. Therefore, based on the observation of an obvious downward deviation in $1/\chi(T)$ curve and a pronounced variation in EPR spectra at 380 K, we can consider that the Griffiths phase appears in the current nanosized materials. In addition, a small distinction between Fig. 4(d) and(b and c) is worthy of our attention. From 380 to 300 K, both g-factor and ΔH_{PP} show a progressive development with decreasing temperature. However, the DIN values first increase and then tend to saturate. This behavior clearly indicates that the obvious variation of EPR spectra observed in 380 K is not due to superparamagnetic phase, which should cause a temperature dependence DIN according to Langevin function rather than a saturation. Thus, we are certain
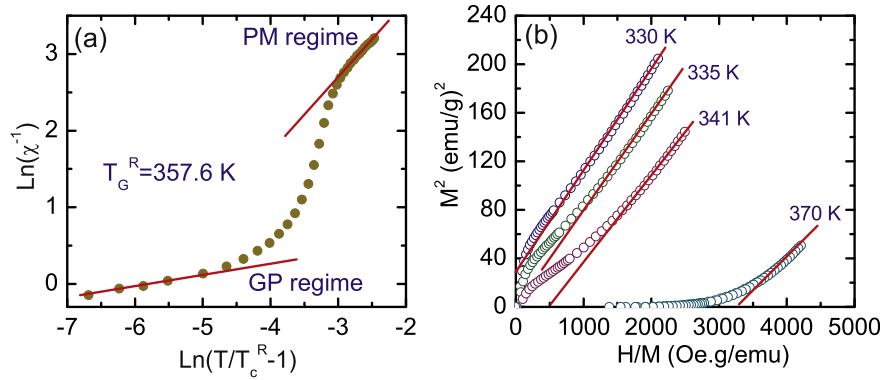
Fig. 5. (a) Susceptibility data are plotted against temperature following Eq. (1) in double natural logarithmic scale. Continuous lines are due to straight line fittings. (b) Arrott plot (M^2 vs H/M) of isotherms collected at different temperatures both below and above T_C are plotted. Lines are due to straight line fitting of plot in high field.

that the confined sample size to nanoscale results in the Griffiths phase in the present system.

Generally, Griffiths singularity is characterized by the exponent λ ($0 \leq \lambda \leq 1$) obtained from the following formula:

$$\chi^{-1} = \left(T - T_G^R\right)^{1-\lambda} \qquad (1)$$

T_G^R is the critical temperature of the random ferromagnet where susceptibility diverges [38,39]. The above equation in fact is the modified Curie–Weiss law where the exponent λ quantifies a deviation from Curie–Weiss behavior and strength of the Griffiths phase. In the pure PM region, λ is expected to be zero. As the temperature decreases from high temperature, more number of clusters achieve FM ordering and the systemical susceptibility tend to diverge at critical temperature T_G^R. Therefore, according to Bray's generalization of bond distribution of Griffiths concept [40], in the temperature range of T_G^R T< T_G, the system is thought to form the Griffiths phase where it neither exhibits pure PM behavior nor long-range FM ordering state. Instead, there exists spatially distributed regions which develops some small FM clusters with different sizes in PM region. Here, the Griffiths singularity can be characterized by utilizing Eq. (1). Fig. 5(a) show the plot of χ^{-1} vs. (T/T_G^R-1) in a ln–ln scale. The two slopes of fitted straight lines in PM state and Griffiths singularity give λ_{PM} and λ_{GP} respectively. The determination of proper λ is very sensitive to the selected value of T_G^R. An incorrect value of T_G^R will lead to an erroneous λ. We have followed a rigorous method prescribed in Ref. 21 to choose a suitable T_G^R. As listed in Table 1, the obtained value of T_G^R is found to be 357.6 K which is the most appropriate value to guarantee the fitting λ_{PM} as small as possible in the current system. Actually, T_G^R should be very close to the Weiss temperature T_{CW} because λ_{PM} becomes nearly zero in the pure PM region. Here the obtained $T_G^R = 357.6$ K is basically consistent with $T_{CW} = 356.5$ K deduce from the fitting inverse susceptibility curve in Fig. 2, indicating that T_G^R determinated with above method is reasonable. Moreover, the obtained $\lambda_{GP} = 0.7552$ in Griffiths phase region is also quite comparable with that for other manganites [41–43]. So, the current experimental results further verify that a Griffiths singularity emerges in the La$_{0.5}$

Sr$_{0.5}$ MnO$_3$ nanoparticles. In the region of Griffiths singularity, the short range correlated embedded FM clusters exist in PM matrix but these clusters do not form long rang FM ordering. Hence, the system does not exhibit spontaneous magnetization(M_S). It can be verified with the Arrott plot (M^2 vs. H/M) which is transferred from the isothermal magnetization curve (M vs. H). Positive intercepts on M^2 axis of the high field extrapolation of Arrott plot correspond to M_S. As shown in Fig. 5(b), until to T = 341 K, we do not find any positive intercepts on M^2 axis indicating no spontaneous magnetization exists above T = 341 K. (only four isotherms curves are shown for clarity). Thus, it confirms the absence of spontaneous magnetization and long range FM ordering in the Griffiths phase regime T_G^R< T< T_G.

In order to understand the Griffiths singularity emerged in La$_{0.5}$ Sr$_{0.5}$ MnO$_3$ nanoparticles, we use core–shell model and the following scenario to account for it [15,16,44]. For the bulk material, its average size of the grains usually reaches above micrometer scale. The number of interacting cluster per grain is very large. In this situation, the main properties of materials are decided by these interacting clusters (from core) instead of the surface effect or topology structure of grain (from shell). As the average size of the grain is confined to nanometer scale, the number of interacting cluster per grain becomes very small and even countable. In this case, the magnetic behavior will be apt to form a relatively larger fluctuation due to the decreasing interaction between the neighboring clusters. At the same time, the reduction in grain size amount to increase the ratio of surface to volume. Therefore, the interaction from shell becomes a main factor to dominate the material properties. Consider a fact that the disorder effect is prerequisite for the formation of Griffiths singularity, we think the increasing surface disorder is direct reason for the presence of Griffiths singularity. Why does surface disorder appear and increase? Under nanoscale, the inner interaction can not completely restrain the behaviors of each members. So, every cluster has large flexibility and even freely rotates. Thus, the magnetic exchange interactions show an obvious random spatial variation. Together with the increase of surface spin due to the reduction in grain size, the local FM fluctuations are easy to form and in turn lead to the presence of Griffiths singularity in the present material at the temperature far above T_C.

4. Conclusion

In summary, we have fabricated La$_{0.5}$ Sr$_{0.5}$ MnO$_3$ nanoparticles by sol–gel method and studied the magnetic phase transition. The mean particle size was determined to be about 100 nm from the observation of SEM and analysis of XRD with Scherrer formulation.

Table 1
Curie temperature T_C, Weiss temperature T_{CW}, Griffiths temperature T_G, Critical temperature T_G^R, and the inverse susceptibility exponents (λ) in PM and Griffiths regime.

Sample	T_C(K)	T_{CW}(K)	T_G(K)	T_G^R(K)	λ_{PM}	λ_{GP}
LSMO	340	356.5	378	357.6	0.0185	0.7552

The temperature dependence inverse susceptibility exhibits a possible Griffiths singularity occurred at the temperature far above T_C. The existence of Griffiths singularity was confirmed by the EPR analysis. We think that the emergence of Griffiths singularity is mainly due to the formation of surface spin disordering in nano-scale process.

Acknowledgment

References

[1] R. von Helmolt, J. Wecker, B. Holzapfel, L. Schultz, K. Samwer, Phys. Rev. Lett. 71 (1993) 2331.
[2] S. Jin, T.H. Tiefel, M. McCormack, R.A. Fastnacht, R. Ramesh, L.H. Chen, Science 264 (1994) 413.
[3] S. Mori, C.H. Chen, S.-W. Cheong, Nat. Lond. 392 (1998) 473.
[4] C.N.R. Rao, A.K. Cheetham, Science 276 (1999) 911.
[5] Y. Tokura, N. Nagaosa, Science 288 (2000) 462.
[6] A.M.L. Lopes, J.P. AraÚjo, V.S. Amaral, J.G. Correia, Y. Tomioka, Y. Tokura, Phys. Rev. Lett. 100 (2008) 155702.
[7] H.Y. Zhai, J.X. Ma, D.T. Gillaspie, X.G. Zhang, E.W. Plummer, J. Shen, Phys. Rev. Lett. 97 (2006) 167201.
[8] M. Moya, L.E. Hueso, F. Maccherozzi, A.I. Tovstolytkin, D.I. Podyalovskii, C. Ducati, L.C. Phillips, M. Ghidini, O. Hovorka, A. berger, M.E. Vickers, E. Defay, S.S. Dhesi, N.D. Mathur, Nat. Mater 12 (2013) 52.
[9] P. Dey, T.K. Nath, Appl. Phys. Lett. 89 (2006) 163102.
[10] B. Roy, A. Poddar, S. Das, J. Appl. Phys. 100 (2006) 104318.
[11] S.M. Zhou, Y.Q. Guo, J.Y. Zhao, L.F. He, C.L. Wang, L. Shi, J. Phys. Chem. C 115 (2011) 11500.
[12] S. Kundu, T.K. Nath, J. Appl. Phys. 111 (2012) 113903.
[13] P. Lampen, N.S. Bingham, M.H. Phan, H. Kim, M. Osofsky, A. Piqué, T.L. Phan, S.C. Yu, H. Srikanth, Appl. Phys. Lett. 102 (2013) 062414.
[14] Yue Ying, Jiyu Fan, Li Pi, Zhe Qu, Wenqing Wang, Bo Hong, Shun Tan, Yuheng Zhang, Phys. Rev. B 74 (2005) 144433.
[15] S. Dong, F. Gao, Z.Q. Wang, J.M. Liu, Z.F. Ren, Appl. Phys. Lett. 90 (2007) 082508.
[16] R.N. Bhowmik, R. Nagarajan, R. Ranganathan, Phys. Rev. B 69 (2004) 054430.
[17] J.M. De Teresa, M.R. Ibarra, P.A. Algarabel, C. Ritter, C. Marquina, J. Blasco, J. Garcia, A. del Moral, Z. Arnold, Nature 386 (1997) 256.
[18] C. He, M.A. Torija, J. Wu, J.W. Lynn, H. Zheng, J.F. Mitchell, C. Leighton, Phys. Rev. B 76 (2007) 014401.
[19] J. Deisenhofer, D. Braak, H.A. Krug von Nidda, J. Hemberger, R.M. Eremina, V.A. Ivanshin, A.M. Balbashov, G. Jug, A. Loidl, T. Kimura, Y. Tokura, Phys. Rev. Lett. 95 (2005) 257202.
[20] C. Magen, P.A. Algarabel, L. Morellon, J.P. Araújo, C. Ritter, M.R. Ibarra, A.M. Pereira, A. Loidl, J.B. Sousa, Phys. Rev. Lett. 96 (2006) 167201.
[21] Jiyu Fan, Li Pi, Yan He, Langsheng Ling, Jixia Dai, Yuheng Zhang, J. Appl. Phys. 101 (2007) 123910.
[22] A.K. Pramanik, A. Banerjee, Phys. Rev. B 81 (2010) 024431.
[23] R.B. Griffiths, Phys. Rev. Lett. 23 (1969) 17.
[24] M.T. Causa, M. Tovar, A. Caneiro, F. Prado, G. Ibañez, C.A. Ramos, A. Butera, B. Alascio, X. Obradors, S. Piñol, F. Rivadulla, C. Vázquez-Vázquez, M.A. López-Quintela, J. Rivas, Y. Tokura, S.B. Oseroff, Phys. Rev. B 58 (1998) 3233.
[25] M.S. Seehra, M.M. Ibrahim, V.S. Babu, G. Srinivasan, J. Phys. Condens. Matter 8 (1996) 11283.
[26] S. Angappane, M. Pattabiraman, G. Rangarajan, K. Sethupathi, V.S. Sastry, Phys. Rev. B 69 (2004) 094437.
[27] Jiyu Fan, Wei Tong, Lei Zhang, Yangguang Shi, Yan Zhu, Dazhi Hu, Weichun Zhang, Yao Ying, Langsheng Ling, Li Pi, Yuheng Zhang, Phys. Status Solidi B 249 (2012) 1634.
[28] E. Rozenberg, M. Auslender, A.I. Shames, Ya.M. Mukovskii, E. Sominski, A. Gedanken, J. Appl. Phys. 105 (2009) 07D707.
[29] E. Rozenberg, A.I. Shames, M. Auslender, Nanosci. Nanotech. Lett. 3 (2011) 531.
[30] V. Likodimos, M. Pissas, Phys. Rev. B 76 (2007) 024422.
[31] A. Shengelaya, G.M. Zhao, H. Keller, K.A. MÜller, Phys. Rev. Lett. 77 (1996) 5296.
[32] S.B. Oseroff, M. Torikachvili, J. Singley, S. Ali, S.-W. Cheong, S. Schultz, Phys. Rev. B 53 (1996) 6521.
[33] F. Rivadulla, M.A. Lopez-Quintela, L.E. Hueso, J. Rivas, M.T. Causa, C.A. Ramos, R.D. Sanchez, M. Tovar, Phys. Rev. B 60 (1999) 11922.
[34] J. Yang, X. Rong, D. Suterc, Y.P. Sun, Phys. Chem. Chem. Phys. 13 (2011) 16343.
[35] Jiyu Fan, Langsheng Ling, Bo Hong,Wei Tong,Lei Zhang, Yangguang Shi, Weichun Zhang, Yan Zhu, Dazhi Hu,Yao Ying, Li Pi, Yuheng Zhang, Appl. Phys. A 112 (2013) 397.
[36] D.L. Huber, G. Alejandro, A. Caneiro, M.T. Causa, F. Prado, M. Tovar, S.B. Oseroff, Phys. Rev. B 60 (1999) 12155.
[37] D.L. Huber, J. Phys. Condens. Matter 26 (2014) 056002.
[38] A.H. Castro Neto, G. Castilla, B.A. Jones, Phys. Rev. Lett. 81 (1998) 3531.
[39] M.B. Salamon, P. Lin, S.H. Chun, Phys. Rev. Lett. 88 (2002) 197203.
[40] A.J. Bray, Phys. Rev. Lett. 59 (1987) 586.
[41] Z.W. Ouyang, V.K. Pecharsky, K.A. Gschneidner Jr., D.L. Schlagel, T.A. Lograsso, Phys. Rev. B 74 (2006) 094404.
[42] W. Jiang, X.Z. Zhou, G. Williams, Y. Mukovskii, K. Glazyrin, Phys. Rev. Lett. 99 (2007) 177203.
[43] E.V. Sampathkumaran, N. Mohapatra, S. Rayaprol, K.K. Iyer, Phys. Rev. B 75 (2007) 052412.
[44] V.M. Andrade, R.J. Caraballo-Vivas, T. Costas-Soares, S.S. Pedro, D.L. Rocco, M.S. Reis, A.P.C. Campos, A.A. Coelho, J. Solid State Chem. 219 (2014) 87.